Research Article

Journal of PeptideScience

Received: 17 September 2010 Revised: 28 October 2010 Accepted: 1 November 2010 Published online in Wiley Online Library: 28 December 2010

(wileyonlinelibrary.com) DOI 10.1002/psc.1335

# Self-assembly of amphiphilic β-sheet peptide tapes based on aliphatic side chains‡

**Robert Philip Wynn Davies and Amalia Aggeli***

**Amphiphilic β-sheet nanotapes based on the self-assembly of 9mer and 7mer *de novo* designed β-strand peptides were studied in the dilute regime. The hydrophobic face of the tapes consisted predominantly of aliphatic (leucine) side chains, while the hydrophilic tape face contained polar side chains (glutamine, arginine and glutamic acid). Both peptides underwent a transition from a monomeric random coil to a self-assembled β-sheet tape upon increase of peptide concentration in aqueous solutions. $P_9$-6 exhibited lower critical concentration (c*) for self-assembly and thus higher propensity for self-assembly in water, compared to the shorter $P_7$-6. At neutral pH where there was little net charge per peptide, self-assembly was favoured compared to low pH in which there was a net +1 charge per peptide; the net charge decreased overall intermolecular attraction, manifested as an increase in c* for self-assembly in low compared to neutral pH aqueous solutions. Propensity for self-assembly and β-sheet formation was found to be greatly enhanced in a polar organic solvent (methanol) compared to water. These studies combined with future more extensive comparative studies between amphiphilic tapes based on aliphatic amino acid residues and amphiphilic tapes based on aromatic residues will throw more light on the relative importance of hydrophobic *versus* aromatic interactions for the stabilisation of peptide assemblies. Systematic studies of this kind may also allow us to throw light on the fundamental principles that drive peptide self-assembly and β-sheet formation; they may also lead to a set of refined criteria for the effective design of peptides with prescribed combination of properties appropriate for specific applications. Copyright © 2010 European Peptide Society and John Wiley & Sons, Ltd.**

**Keywords:** self-assembling peptides; β-sheet; biomaterials; amphiphilic peptides

## Introduction

Peptide self-assembly is a ubiquitous phenomenon in nature giving rise to an extensive range of functional or pathological nanostructures [1,2]. In recent years, scientists, inspired from Nature, have embarked on learning how to use self-assembling peptides as versatile, natural and multifunctional building blocks in order to produce a variety of well-defined nanostructures, materials and devices for applications in medicine and nanotechnology [1–9]. In order to develop novel materials and applications based on self-assembling peptides, it is imperative that we acquire a thorough understanding of the principles and forces that govern peptide self-assembly as well as a detailed knowledge of the relationship between peptide primary structure, self-assembly, nanostructure formation and material properties.

One particular novel class of self-assembling peptides, which was previously developed, is based on simple peptides that adopt entirely a β-strand conformation (Figure 1(A)) and self-assemble in one dimension in solution to give rise to β-sheet nanotapes (Figure 1(B)) as well as higher order aggregates: ribbons (Figure 1(C)), fibrils and fibres [10–12]. Solutions and gels made of these peptides are currently explored in a broad range of applications [13–15]. One of the best characterised member of this class of tape-forming peptides is *de novo* designed 11mer peptide $P_{11}$-2 [10,11]. Once aggregated, $P_{11}$-2 gives rise to amphiphilic β-sheet tapes with a hydrophilic face being decorated by polar (glutamine, arginine and glutamic acid) side chains and a hydrophobic face consisting mainly of aromatic (phenylalanine and tryptophan) side chains. Association between aromatic amino acid residues has been hypothesised to be one of the main forces that promotes self-assembly of peptides. Referred to as π–π interactions or π stacking, these attractive interactions occur between planar aromatic rings and it is the direction of the stacking which plays a role in promoting self-assembly [3]. The high occurrence of aromatic residues in amyloid-related peptides, such as islet amyloid, aortic medial amyloid and Alzheimers β-amyloid, has further led to the summation that such residues play a pivotal role in their formation. Extensive studies [16–19] indicated that aromatic moiety plays a vital role in the formation of aggregates. The Px-2 family of tape-forming peptides, including $P_{11}$-2 as well as shorter and longer variants, were also previously designed based on the supposition that the presence of aromatic side chains would increase propensity for self-assembly and stability of the β-sheet tape [10]. More recently, another Px-6 family of tape-forming peptides was designed. The only difference between the peptides in the Px-2 and Px-6 families is that the aromatic side chains of the peptides in Px-2 family have been substituted by aliphatic side chains in the Px-6 family. Thus, the Px-2 family of peptides forms β-sheet tapes whose hydrophobic face consists mainly of aromatic side chains (phenylalanine, tryptophan), while the Px-6 family of peptides forms tapes whose hydrophobic face contains predominantly aliphatic (leucine) side chains.

Here we study the self-assembly in the dilute regime of the first two members of the Px-6 family: 7mer and 9mer peptides $P_7$-6 and

* *Correspondence to: Dr Amalia Aggeli, Centre for Molecular Nanoscience, School of Chemistry, University of Leeds, Leeds LS2 9JT, UK. E-mail: a.aggeli@leeds.ac.uk*

*Centre for Molecular Nanoscience, School of Chemistry, University of Leeds, Leeds LS2 9JT, UK*

‡ *Special issue devoted to contributions presented at the E-MRS Symposium C "Peptide-based materials: from nanostructures to applications", 7-11 June 2010, Strasbourg, France.*

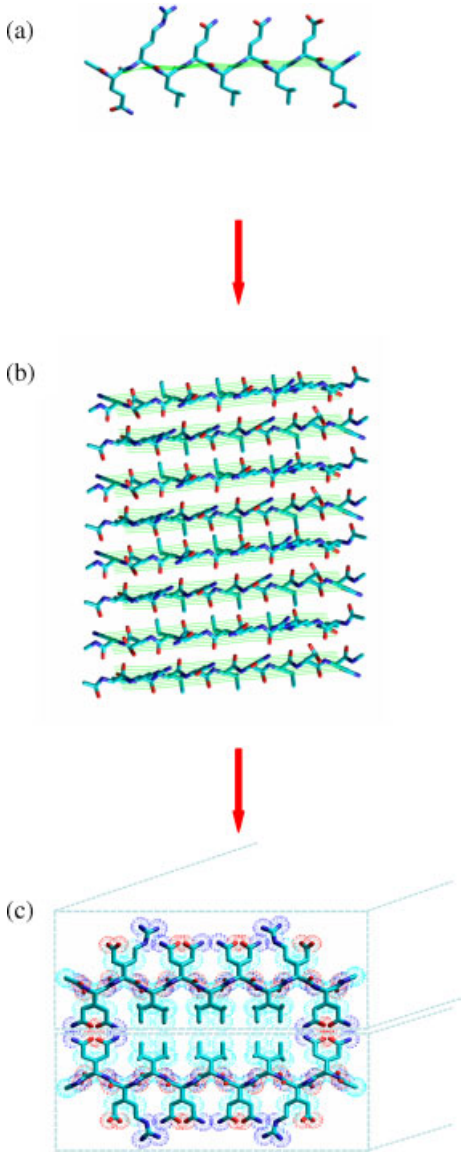


**Figure 1.** (A) $P_9$-6 in a $\beta$-strand conformation; (B) top view of one-dimensional self-assembly of $P_9$-6 $\beta$-strands in order to produce a $\beta$-sheet tape; (C) cross section of two tapes stacked on top of each other via their hydrophobic faces that are decorated by the aliphatic side chains. (A), (B) and (C) were drawn using HyperChem7, and are intended as a schematic. This figure is available in colour online at wileyonlinelibrary.com/journal/jpepsci.

$P_9$-6 (Table 1), using CD-UV spectroscopy and TEM microscopy. These investigations as well as future extensive comparative studies between Px-6 and Px-2 families will help decipher the role of aromatic *versus* aliphatic interactions in the stabilisation of peptide self-assembly and $\beta$-tape formation.

## Materials and Methods

### Peptide Synthesis, Purification and Quality Control

Peptides were synthesised in-house as described previously [20] and purified by HPLC. Peptide quality control was undertaken using mass spectroscopy, analytical HPLC, amino acid and elemental analysis (carbon, hydrogen, nitrogen and fluorine) and

**Table 1.** Peptide primary structures

| Peptide | Primary structure |
|---|---|
| $P_7$-6 | $CH_3CO$-RLQLQLE-$NH_2$ |
| $P_9$-6 | $CH_3CO$-**Q**RLQLQLE**Q**-$NH_2$ |

UV spectroscopy with the following results: $P_9$-6 (theoretical mass: 1197.39 Da, 87% peptide content) and $P_7$-6 (theoretical mass: 940.52 Da, 84% peptide content). The peptide content reflects non-peptide molecules present in the dry peptide mass; these were mainly residual amounts of water, ammonium counterions bound on negatively charged peptide groups and trifluoroacetic acid counterions bound on positively charged groups. All peptides were stored at −20 °C as freeze-dried white fluffy powders.

### Circular Dichroism (CD) UV Spectrometry

CD-UV spectra were acquired using a JASCO 715 spectrometer. Peptide solutions were prepared by initially producing a 5 mg/ml stock solution. Aliquots of this solution were then added to an

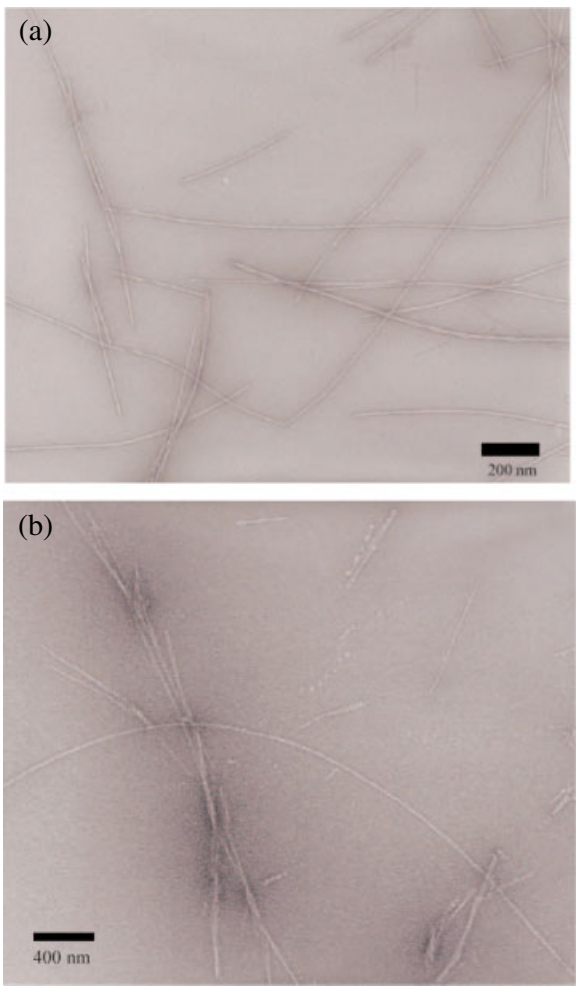


**Figure 2.** TEM micrograph of (A) $P_7$-6 in water after 19 days of incubation at a concentration of 700 μM and (B) $P_9$-6 in water after 12 days of incubation at a concentration 260 μM. This figure is available in colour online at wileyonlinelibrary.com/journal/jpepsci.



  

Journal of PeptideScience

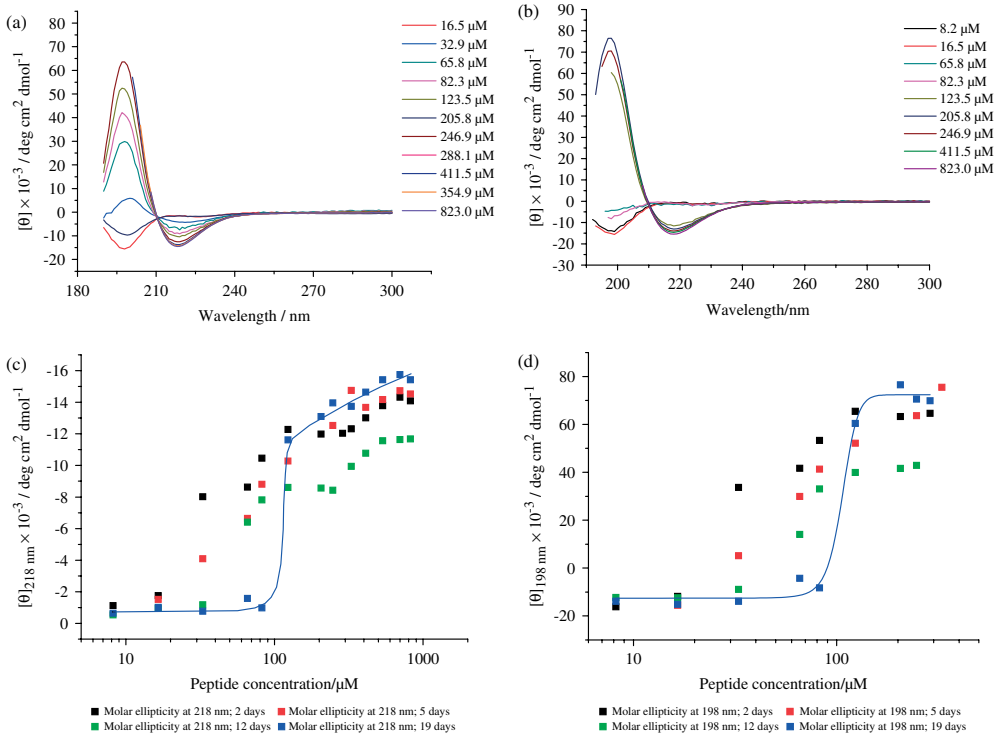


**Figure 3.** CD-UV spectra of $P_7$-6 in near-neutral water (pH 6.5 $\pm$ 0.7) as a function of peptide concentration and incubation time, after (A) 5 days and (B) 19 days of incubation time. (C) A plot of the mean residue molar ellipticity of $P_7$-6 at 218 nm in water as a function of peptide concentration and incubation time; the solid line indicates the apparent equilibrium state of the solutions. (D) A plot of the mean residue molar ellipticity of $P_7$-6 at 198 nm in water as a function of peptide concentration and incubation time; the solid line indicates the apparent equilibrium state of the solutions. The solid lines are there to guide the eye and not the result of fitting of the data with the theoretical model that describes peptide self-assembly.

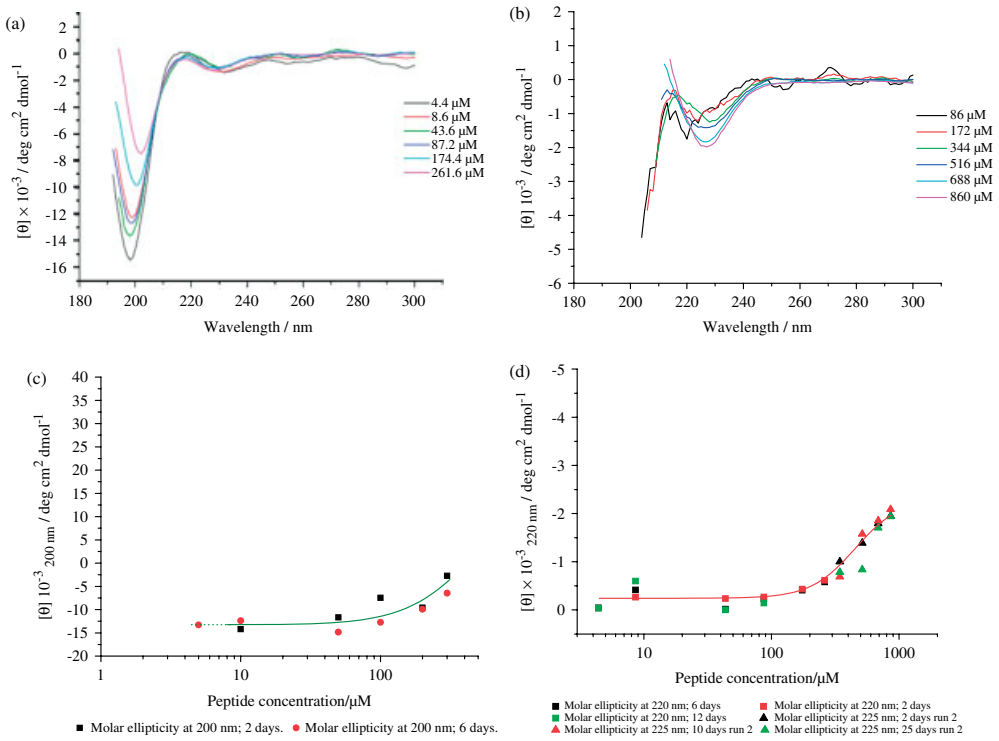


**Figure 4.** CD-UV spectra of $P_7$-6 in water at pH 2 with 10 mM orthophosphoric acid as a function of peptide concentration and incubation time after (A) 2 days and (B) 6 days of incubation time. (C) A plot of the mean residue molar ellipticity of $P_7$-6 at 200 nm in pH 2 as a function of peptide concentration and incubation time; the solid line indicates the apparent equilibrium state of the solutions. (D) A plot of the mean residue molar ellipticity of $P_7$-6 at 220 nm in pH 2 as a function of peptide concentration and incubation time; the solid line indicates the apparent equilibrium state of the solutions. The solid lines are there to guide the eye and not the result of fitting of the data with the theoretical model that describes peptide self-assembly.



  

appropriate amount of solvent to produce specific concentrations. A 1 nm bandwidth with a step resolution of 1 nm was used to acquire 10 scans per sample over a range of 190–300 nm. The resulting data were then baseline corrected, smoothened and normalised.

### Transmission Electron Microscopy

Samples were placed on copper EM grids with a mesh size of 400, which were coated with glow discharged carbon film. A droplet of undiluted peptide solution was deposited onto the grid (~1 min), the excess was removed, and the samples were left to air dry. The grids were then negatively stained with uranyl acetate solution (4% w/v) for 20 s and air-dried. TEM images were collected using a Philips CM10 TEM at 80 kV accelerating voltage.

## Results and Discussion

Both $P_9$-6 and $P_7$-6 (Table 1) were found to self-assemble and give rise to self-supporting gels in aqueous solutions with peptide concentration in the mg/ml range. The gel was seen to be the result of a three-dimensional network of well-defined, elongated, semi-rigid, nanostructures with typical width of 11–17 nm, persistence length of hundreds of nanometres and full length ranging from 0.1 to several μm, as revealed by transmission electron microscopy (Figure 2). The width and rather rigid appearance of these nanostructures are in agreement with them being nanofibrils of approximately 10–16 stacked and twisted $\beta$-sheet tapes (Figure 1(B)) or – five to eight ribbons (pair of stacked tapes) (Figure 1(C)) per fibril. The self-assembly of both peptides was studied and compared in detail in the dilute regime as a function of peptide concentration using CD-UV spectroscopy and in three different solvents: pure water at near-neutral pH, and water at pH 2 were used to decipher peptide self-assembly in an aqueous environment and at pHs in which the peptides carry different amount of charge, while self-assembling studies in methanol were also carried out in order to investigate the effect of decreased relative dielectric constant on peptide self-assembly.

### Self-assembly of $P_7$-6

The self-assembly of $P_7$-6 in water (pH 6.5 $\pm$ 0.7) was followed as a function of time by CD-UV spectroscopy (Figure 3). At this pH, both arginine and glutamic acid side chains carry their respective positive and negative charges, thus the peptide has very little net charge (Table 1). Solutions of increasing peptide concentration were prepared and left to equilibrate for 5 days at 20 °C, after which point they were studied by CD-UV spectroscopy (Figure 3(A)). Low concentrations, e.g. 16.5 μM, show spectra with a negative minimum centreed at 198 nm, characteristic of monomeric, random coil peptides. Upon increase of peptide concentration, a positive band at 198 nm and a negative band at 218 nm develop gradually, which are diagnostic of $\beta$-sheet structure. Thus, the peptide converts from a monomeric random coil to a self-assembled $\beta$-sheet state upon increase of peptide concentration. For solutions equilibrated for 5 days, the critical concentration (c*) for the monomer to aggregate transition was found to be roughly at *ca* 20 μM. In order to establish the equilibrium state of the peptide solutions, the samples were examined as a function of time after incubation for 2, 5 (Figure 3(A)), 12 and 19 days (Figure 3(B)) from sample preparation. The molar ellipticities of the two bands at 198 and 218 nm were plotted as a function of peptide concentration and incubation time of the solutions (Figure 3(C) and (D)). It thus becomes obvious that the solutions and thus the molar ellipticities keep changing with time and it takes a rather long time, specifically approximately 2.5 weeks for the solutions to reach an apparent equilibrium state shown by the solid lines in Figure 3(C) and (D). At equilibrium, the c* for self-assembly of $P_7$-6 peptide in water appears to be roughly at 80 μM based on the positive band at 198 nm (Figure 3(D)) and at about 100 μM (Figure 3(C)) based on the negative band at 218 nm. This discrepancy is most likely due to the higher sensitivity of the $\beta$-sheet band at 198 nm because it is a lot stronger (higher molar extinction coefficient) compared to the $\beta$-sheet band at 218 nm. On the basis of these studies, it is recommended whenever possible to obtain peptide self-assembly data based primarily on the positive band at 198 rather than the negative band at 218 nm, because the former seems to be a more sensitive indicator of self-assembly than the latter. Another interesting observation is that there is not a single isodichroic point for all collected CD spectra at long incubation times (e.g. Figure 3(A) and (B)), while there is a single isodichroic point in all collected CD spectra after 2 days of incubation, which implies a simple two-state transition; this suggests a more complex self-assembly in longer time scales, involving more than two distinct states. This is in agreement with the hierarchical self-assembly model, in which the tapes and ribbons form first from monomers and subsequently they become the building blocks for formation of higher order structures i.e. fibrils and fibres.

Self-assembly of $P_7$-6 was also studied in water at pH 2.0 (Figure 4), following the same approach as above. At this pH, arginine is positively charged, while glutamic acid is neutral, thus the peptide carries a net +1 charge (Table 1). It is obvious from the CD spectra (Figure 4(A)) that there is no visible positive $\beta$-sheet band at 198 nm, coupled with only a weak negative $\beta$-sheet band at 218 nm only apparent at fairly high peptide concentrations (Figure 4(B)). Thus, at pH 2.0 the peptide has a much higher tendency to remain in monomeric random coil state rather than at pH 6.5. The molar ellipticities of the bands at 200 nm (Figure 4(C)) and 220 nm (Figure 4(D)) were plotted as a function of peptide concentration and incubation time of the samples. At apparent equilibrium at pH 2.0 (solid lines in Figure 4(C) and (D)), c* for self-assembly seems to be roughly at 130 μM (compared with *ca* 80 μM at pH 6.5) based on the stronger band at 200 nm and approximately at 250 μM (compared to *ca* 100 μM in pH 6.5) based on the weaker $\beta$-sheet band at 220 nm. The +1 net charge on the peptide at pH 2.0 is most likely causing increased repulsion between peptides compared to pH 6.5; this can explain the increased c* for self-assembly at low compared to near neutral pH. Thus, it is expected that the higher the net charge per peptide, the higher its c* for self-assembly and the lower its propensity for self-assembly.

There is a lot of interest in understanding peptide self-assembly not only in water but also in organic solvents. This can tell us about the likely effect of a more hydrophobic environment on peptide self-assembly; it can also expand the range of applications that these peptides can be explored for. In the present studies, methanol was used as a model organic solvent to study peptide self-assembly. At all concentrations studied in methanol, the peptide was found to self-assemble into $\beta$-sheet structures as is evident from the negative band at *ca* 224 nm and the positive band at *ca* 200 nm (Figure 5(A)). The situation did not change as a function of time. Thus, at equilibrium c* for self-assembly in methanol seems to be a lot lower than 4 μM



  

Journal of PeptideScience

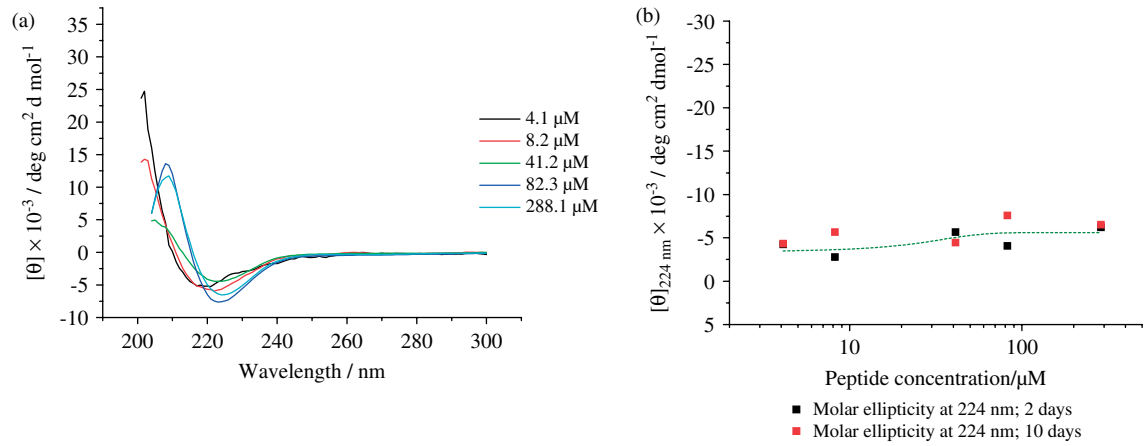


**Figure 5.** CD-UV spectra of $P_7$-6 in methanol as a function of peptide concentration and incubation time, after (A) 10 days. (B) Mean residue molar ellipticity at 224 nm of $P_7$-6 in methanol after 2 and 10 days as a function of peptide concentration. The dotted line is there to guide the eye and not the result of fitting of the data with the theoretical model that describes peptide self-assembly.

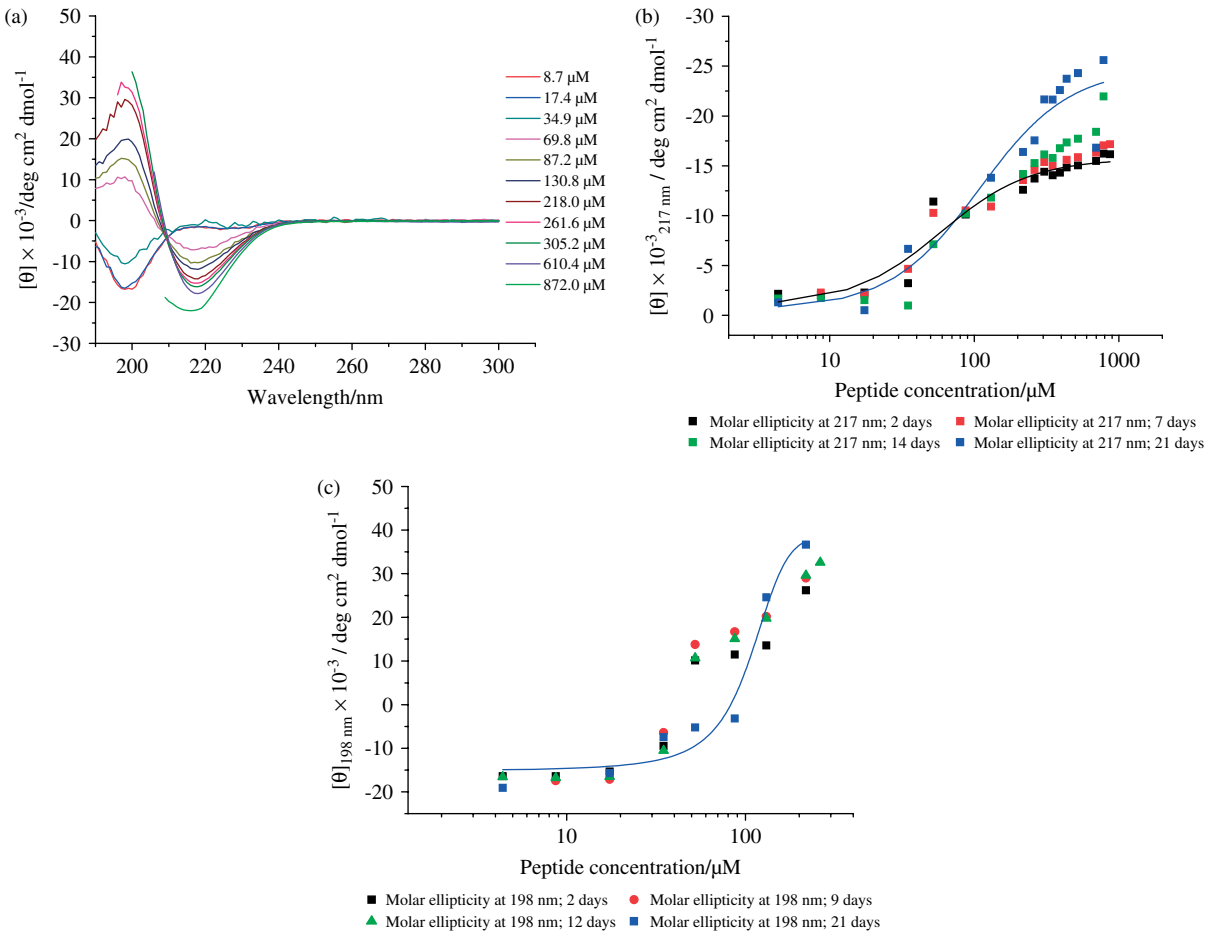


**Figure 6.** CD-UV spectra of $P_9$-6 in water at near-neutral pH (6.7 $\pm$ 0.5) as a function of peptide concentration and incubation time, after (A) 14 days of incubation time. (B) A plot of the mean residue molar ellipticity of $P_9$-6 at 217 nm in water as a function of peptide concentration and incubation time; the blue solid line indicates the apparent equilibrium state of the solutions. (C) A plot of the mean residue molar ellipticity of $P_9$-6 at 198 nm in water as a function of peptide concentration and incubation time; the blue solid line indicates the apparent equilibrium state of the solutions. The solid lines are there to guide the eye and not the result of fitting of the data with the theoretical model that describes peptide self-assembly.



  

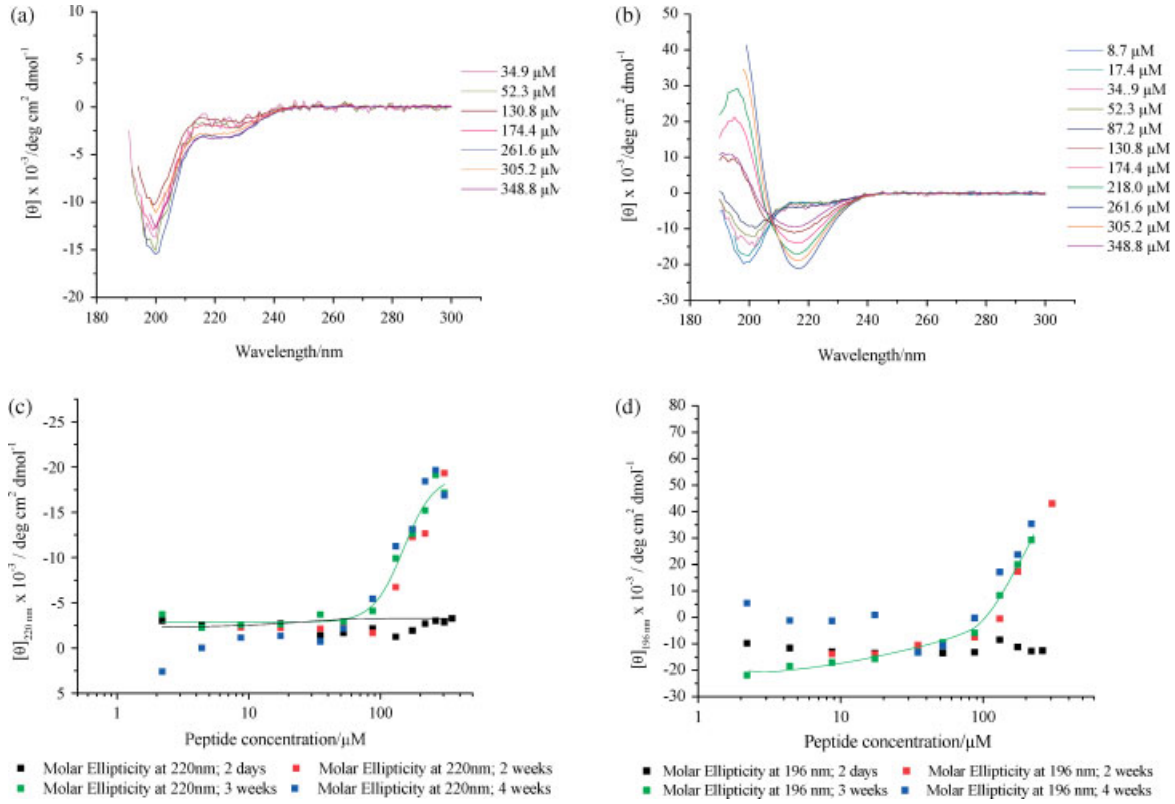


**Figure 7.** CD-UV spectra of $P_9$-6 in water at pH 2 with 10 mM orthophosphoric acid as a function of peptide concentration and incubation time after (A) 2 days and (B) 3 weeks of incubation time. (C) A plot of the mean residue molar ellipticity of $P_9$-6 at 220 nm in pH 2 as a function of peptide concentration and incubation time; the green solid line indicates the apparent equilibrium state of the solutions, while the black solid lines indicate the starting state of the solutions. (D) A plot of the mean residue molar ellipticity of $P_9$-6 at 196 nm in pH 2 as a function of peptide concentration and incubation time; the green solid line indicates the apparent equilibrium state of the solutions. The solid lines are there to guide the eye and not the result of fitting of the data with the theoretical model that describes peptide self-assembly.

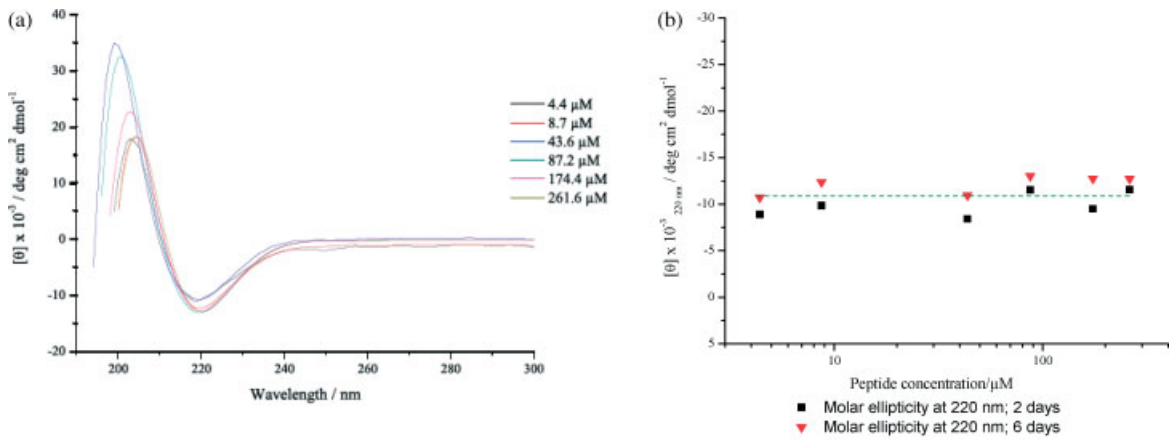


**Figure 8.** CD-UV spectra of $P_9$-6 in methanol as a function of peptide concentration after (A) 2 days of incubation. (B) Mean residue molar ellipticity at 220 nm of $P_9$-6 in methanol after 2 and 6 days of incubation as a function of peptide concentration. The dotted line is there to guide the eye and not the result of fitting of the data with the theoretical model that describes peptide self-assembly.

which is the lowest concentration studied (Figure 5(B)); this is in marked contrast to c* in water at pH 2.0 (*ca* 130 μM) and c* in water at pH 6.5 (*ca* 80 μM). Thus, among the three solvent conditions studied here, a low relative dielectric constant solvent (methanol) gives the lowest c* i.e. it favours most self-assembly into $\beta$-sheets, while aqueous conditions where the peptide has a +1 net charge (pH 2) gives the highest c*, i.e. it favours least self-assembly into $\beta$-sheet. The lower the relative dielectric constant, the higher the intermolecular hydrogen bonding strength that mainly stabilises the $\beta$-sheet tape; this can explain the stabilising effect of the less polar organic solvent (methanol) on the $\beta$-sheet, compared to the aqueous environment. Another likely explanation for this observation is that the solvent competes less effectively with interpeptide hydrogen bonding in the case of methanol compared to water, thus leading to greater stabilisation of the aggregate in methanol compared to water.



  

Journal of PeptideScience

### Self-assembly of $P_9$-6

A comparative study to $P_7$-6 was also carried out with the longer peptide variant $P_9$-6 in order to examine the consistency/generality of our conclusions with $P_7$-6 and to also start deciphering the effect of the length of the peptide $\beta$-strand on the self-assembly process. $P_9$-6 was first studied at near-neutral pH ($6.7 \pm 0.5$) in water as a function of increasing peptide concentration and incubation time of the samples (Figure 6). A clear transition was again observed as in $P_7$-6, from a random coil monomer at low concentrations to a $\beta$-sheet structure at higher concentrations. The apparent equilibrium conditions of the samples were reached after a couple of weeks of incubation at 20 °C (solid blue lines in Figure 6(B) and (C)). At equilibrium, the c* for self-assembly of $P_9$-6 appears to be approximately at 30 μM based on the more sensitive band at 198 nm (compared to 80 μM for $P_7$-6 under the same conditions) and roughly at 50 μM based on the less sensitive band at 217 nm (compared to 100 μM for $P_7$-6 under the same conditions). Thus, an increase of peptide length by two amino acid residues has increased the propensity for self-assembly by more than halving the c* for self-assembly. The longer the peptide, the higher the strength of the intermolecular hydrogen bonds that primarily stabilise the $\beta$-sheet tapes, and thus the lower the c* necessary for self-assembly to start.

At low pH (2.0), $P_9$-7 at short incubation times (Figure 7(A)) exhibited a behaviour similar to $P_7$-6 under the same conditions, i.e. a tendency to remain in a predominantly monomeric random coil state. However, over the course of time, the higher concentration solutions underwent an impressive transition to a predominantly $\beta$-sheet state (Figure 7(B), (C) and (D)). The apparent equilibrium conditions were achieved after approximately 3 weeks of incubation. The apparent equilibrium curves are shown in blue solid lines in Figure 7(C) and (D). Accordingly, the equilibrium c* for self-assembly of $P_9$-6 in pH 2 was found to be *ca* 30 μM based on the more sensitive band at 196 nm (compared to 130 μM for $P_7$-6) and 70 μM based on the less sensitive band at 220 nm (compared to 250 μM for $P_7$-6). Once more the longer peptide favours self-assembly significantly more compared to the shorter peptide, with an at least threefold difference in c* for self-assembly between the two peptides. As in $P_7$-6, $P_9$-6 did not give a clear, single isodichroic point for all collected CD data in most conditions studied (Figures 6 and 7), reflecting once more the more complex hierarchical self-assembly followed by these peptides compared to simpler two-state transitions.

Finally, $P_9$-6 self-assembly was also studied in the lower relative dielectric constant methanol (Figure 8). As in $P_7$-6, distinct $\beta$-sheet spectra were obtained at all concentrations (Figure 8(A)) and at all incubation times (Figure 8(B)). Therefore, the c* for self-assembly in methanol is a lot lower than the lowest concentration studied, i.e. less than 4 μM. These studied are in agreement with the corresponding $P_7$-6 studies.

## Conclusions

Amphiphilic $\beta$-sheet nanotapes were studied, based on the self-assembly of 9mer and 7mer *de novo* designed $\beta$-strand peptides. Aliphatic leucine side chains were mostly positioned on the hydrophobic face of the tapes, while polar glutamine, arginine and glutamic acid side chains were positioned on the polar face of the tapes. Both peptides underwent a transition from a monomeric random coil at low peptide concentration to a self-assembled $\beta$-sheet tape at higher concentrations in aqueous solutions, as monitored by CD-UV spectroscopy. $P_9$-6 exhibited lower critical concentration for self-assembly in water compared to the shorter $P_7$-6, and thus higher propensity for self-assembly compared to $P_7$-6. At neutral pH where there was little net charge per peptide, self-assembly was favoured compared to low pH in which there was a net +1 charge per peptide; this +1 net charge decreased overall intermolecular attraction which was exhibited as an increase in the critical concentration for self-assembly in low pH compared to neutral pH aqueous solutions. The presence of a polar organic solvent (methanol) greatly enhanced propensity for self-assembly and $\beta$-sheet formation, to the extent that the critical concentration for self-assembly in methanol was significantly lower than the lowest concentration studied by CD-UV spectroscopy. Further comparative studies that are currently taking place, between amphiphilic tapes based on aliphatic amino acid residues and amphiphilic tapes based on aromatic residues, will throw more light on the relative importance of hydrophobic *versus* aromatic interactions for the stabilisation of peptide assemblies. Systematic studies of this kind may allow us to piece together the fundamental principles that drive peptide self-assembly and $\beta$-sheet formation; they may also lead to a more detailed set of refined and effective criteria for the design of peptides with well-defined combination of self-assembling and material properties appropriate for specific applications.

### Acknowledgements

Funding for this work was provided by the School of Chemistry, University of Leeds. A. Aggeli gratefully acknowledges the support of the Royal Society through personal Royal Society University Research Fellowship. The work was also partly supported by the WELMEC Centre of Excellence in Medical Engineering funded by the Wellcome Trust and EPSRC, WT088908/z/09/z.

## References

1 Iconomidou VA, Hamodrakas SJ. Natural protective amyloids. *Curr. Protein Pept. Sci.* 2008; **9**: 291–309.
2 Morgan C, Colombres M, Nunez MT, Inestrosa NC. Structure and function of amyloid in Alzheimer's disease. *Prog. Neurobiol.* 2004; **74**: 323–349.
3 Yemini M, Reches M, Rishpon J, Gazit E. Novel electrochemical biosensing platform using self-assembled peptide nanotubes. *Nano Lett.* 2005; **5**: 183–186.
4 Zhang SG, Gelain F, Zhao XJ. Designer self-assembling peptide nanofiber scaffolds for 3D tissue cell cultures. *Semin. Cancer Biol.* 2005; **15**: 413–420.
5 Webber MJ, Kessler JA, Stupp SI. Emerging peptide nanomedicine to regenerate tissues and organs. *J. Intern. Med.* 2010; **267**: 71–88.
6 Gungormus M, Branco M, Fong H, Schneider JP, Tamerler C, Sarikaya M. Self assembled bi-functional peptide hydrogels with biomineralization-directing peptides. *Biomaterials* 2010; **31**: 7266–7274.
7 Rajagopal K, Lamm MS, Haines-Butterick LA, Pochan DJ, Schneider JP. Tuning the pH responsiveness of beta-hairpin peptide folding, self-assembly, and hydrogel material formation. *Biomacromolecules* 2009; **10**: 2619–2625.
8 Zhou M, Smith AM, Das AK, Hodson NW, Collins RF, Ulijn RV, Gough JE. Self-assembled peptide-based hydrogels as scaffolds for anchorage-dependent cells. *Biomaterials* 2009; **30**: 2523–2530.
9 Scanlon S, Aggeli A. Self-assembling peptide nanotubes. *Nano Today* 2008; **3**: 22–30.
10 Aggeli A, Bell M, Boden N, Keen JN, McLeish TCB, Nyrkova I, Radford SE, Semenov A. Engineering of peptide beta-sheet nanotapes. *J. Mater. Chem.* 1997; **7**: 1135–1145.
11 Aggeli A, Nyrkova IA, Bell M, Harding R, Carrick L, McLeish TCB, Semenov AN, Boden N. Hierarchical self-assembly of chiral rod-like



  

molecules as a model for peptide beta-sheet tapes, ribbons, fibrils, and fibers. *Proc. Natl. Acad. Sci. U.S.A.* 2001; **98**: 11857–11862.
12 Davies RPW, Aggeli A, Beevers AJ, Boden N, Carrick LM, Fishwick CWG, McLeish TCB, Nyrkova I, Semenov AN. Self-assembling beta-sheet tape forming peptides. *Supramol. Chem.* 2006; **18**: 435–443.
13 Kirkham J, Firth A, Vernals D, Boden N, Robinson C, Shore RC, Brookes SJ, Aggeli A. Self-assembling peptide scaffolds promote enamel remineralization. *J. Dent. Res.* 2007; **86**: 426–430.
14 Bell CJ, Carrick LM, Katta J, Jin ZM, Ingham E, Aggeli A, Boden N, Waigh TA, Fisher J. Self-assembling peptides as injectable lubricants for osteoarthritis. *J. Biomed. Mater. Res. A* 2006; **78A**: 236–246.
15 Meegan JE, Aggeli A, Boden N, Brydson R, Brown AP, Carrick L, Brough AR, Hussain A, Ansell RJ. Designed self-assembled beta-sheet peptide fibrils as templates for silica nanotubes. *Adv. Funct. Mater.* 2004; **14**: 31–37.
16 Tjernberg LO, Naslund J, Lindqvist F, Johansson J, Karlstrom AR, Thyberg J, Terenius L, Nordstedt C. Arrest of beta-amyloid fibril formation by a pentapeptide ligand. *J. Biol. Chem.* 1996; **271**: 8545–8548.
17 Balbach JJ, Ishii Y, Antzutkin ON, Leapman RD, Rizzo NW, Dyda F, Reed J, Tycko R. Amyloid fibril formation by A beta(16–22), a seven-residue fragment of the Alzheimer's beta-amyloid peptide, and structural characterization by solid state NMR. *Biochemistry* 2000; **39**: 13748–13759.
18 Tenidis K, Waldner M, Bernhagen J, Fischle W, Bergmann M, Weber M, Merkle ML, Voelter W, Brunner H, Kapurniotu A. Identification of a penta- and hexapeptide of islet amyloid polypeptide (IAPP) with amyloidogenic and cytotoxic properties. *J. Mol. Biol.* 2000; **295**: 1055–1071.
19 Mucchiano G, Cornwell GG, Westermark P. Senile aortic amyloid – evidence for 2 distinct forms of localized deposits. *Am. J. Pathol.* 1992; **140**: 871–877.
20 Aggeli A, Bell M, Boden N, Keen JN, Knowles PF, McLeish TCB, Pitkeathly M, Radford SE. Responsive gels formed by the spontaneous self-assembly of peptides into polymeric beta-sheet tapes. *Nature* 1997; **386**: 259–262.

  